LJMU Research Online

García Plaza, E, Chen, X and Ait Ouarab, L

 Grinding Acoustic Emission Features in Relation to Abrasive Scratch Characteristics

http://researchonline.ljmu.ac.uk/id/eprint/13189/

Article

For more information please contact researchonline@ljmu.ac.uk

Grinding Acoustic Emission Features in Relation to Abrasive Scratch Characteristics

Eustaquio García Plaza[1,a] *, Xun Chen[2,b], Lounis Ait Ouarab[2,c]

[1]Higher Technical School of Industrial Engineering, Department Applied Mechanics & Engineering of Projects, University of Castilla-La Mancha, Avda. Camilo José Cela, 13005 Ciudad Real, Spain

[2]Advanced Manufacturing Technology Research Laboratory, General Engineering Research Institute, Liverpool John Moores University, Liverpool L3 3AF, UK.

[a]eustaquio.garcia@uclm.es, [b]X.Chen@ljmu.ac.uk, [c]L.AitOuarab@2016.ljmu.ac.uk

Abstract. On-line monitoring of grinding process has substantial advantages over traditional post-process quality control techniques for detecting malfunctions and reducing costs and inspection times. The selection of appropriate sensors and adequate signal processing methods are essential to establish optimum grinding control strategies with good prediction quality within acceptable response times. This paper assessed three signal-processing methods for grinding surface creation monitoring based on acoustic emission (*AE*) signals in abrasive scratch experiments. The *AE* signals are analysed in time domain (time direct analysis, TDA), frequency domain (fast Fourier transform, FFT) and in the combined time-frequency domain (singular spectrum analysis, SSA). The result showed that the FFT and SSA signal feature extraction methods gives better indication in correlation to the surface creation with different abrasive geometrical characteristics. For both sapphire and zirconia materials, the results of FFT method showed the best correlation between *AE* features and surface creation characteristics in scratching tests and the most significative information was in the frequency range between 0 and 200 kHz. This finding allows a great reduction in the sampling frequency of the signal, making this method the most suitable for real time applications. This work reveals that the *AE* signals processed with the adequate feature extraction method can present good correlation with the characteristics of interaction between abrasive and workpiece in scratching tests and can provide meaningful information for the on-line monitoring of surface creation in grinding processes.

1. Introduction

On-line process monitoring on a CNC machine could bring significant impacts in manufacturing cost and efficiency by reducing post process inspection and rework for product quality control (Lauro et al., 2014; Teti et al., 2010). On line monitoring techniques allows the real time assessing crucial aspects of machining process, such as tool condition (Boaron and Weingaertner, 2018; Arun et al., 2018), chatter (Siddhpura and Paurobally, 2012), surface finish (García and Núñez, 2018), chip formation (Karam and Teti, 2013), and surface damage (Liu et al. 2006; Liu et al., 2005). In order to provide relevant meaningful information, a method of optimum selection of sensors, signal processing algorithms and predictive techniques should be established according to the specified parameters under analysis. A broad range of sensors have been used in machining process monitoring, including dynamometers, accelerometers and acoustic emission sensors (Teti et al., 2010). Considering signal processing, different methods have been applied in time and frequency domain, for example, time direct analysis (TDA) (García et al. 2018), singular spectrum analysis (SSA) (García and Núñez, 2017), Fourier transform (García et al. 2018), and wavelet transform (Liao et al., 2007). For analysing the correlation between various signal parameter features under study, many prediction techniques have been proposed in previous researches, i.e., the multivariate regression (García and Núñez, 2018), the artificial neural networks (García et al., 2018) and the support vector machines (Arun et al., 2018).

Of all machining processes, grinding is one of commonly used processes for finishing operation to achieve tight tolerances and high surface quality of workpieces. In grinding, the wheel surface topography is an important aspect to be evaluated in relation to grinding performance due to the continuously changed abrasive grain shape affects the quality of ground components. In recent years, process monitoring techniques have been extensively investigated and applied to grinding process to monitor critical aspects of grinding process, such as chip thickness (Yang et al., 2019), tool wear (Wegener et al., 2011), surface finish (Nguyen et al., 2019), surface damage (Liu et al., 2006). Nguyen et al. (2019) developed a model to predict the abrasive wear and the surface finish using cutting force signals. The signals were processed in both time and frequency domains so that the wear and the surface finish could be predicted using adaptive neural fuzzy inference system, Gaussian process regression and Taguchi methods. Tang et al. (2009) developed a mathematical model of grinding forces to characterise the surface topography of the ground workpieces. Yang et al. (2019) predicted the minimum chip thickness in single diamond grain grinding using cutting forces, obtaining good relationship between experimental and estimated values.

One of commonly used process signals in grinding monitoring has been acoustic emission (AE), which is defined as an elastic wave propagation in the bandwidth between 20 and 2000 kHz due to material particle displacements under stresses (Lee et al., 2006). The beauty of using AE signal is that AE could provide process dynamic information in much higher frequency domain than other sensors. It also isolates background noise well. In grinding, the acoustic emission signal represents many important aspects of grinding, such as, the rupture of grains and bound bridges in the wheel and the workpiece chipping, cracks, elastic contact, plastic deformation, phase transformation. Thus, AE signals have been used to characterise different technological performance aspect of the grinding process. Griffin and Chen (2009) proposed a method for monitoring phenomena as cutting, ploughing and rubbing in single grit processes using the AE signal. By applying short time Fourier transform it was demonstrated that the three phenomena could be determined in the 50-500 KHz frequency range. Weingaertner and Boaron (2012) monitored the grinding wheel´s topography by analysing the acoustic emission signal in RMS format. Later, Boaron and Weingaertner (2018) analysed acoustic emission signals in both time and frequency domains for evaluating the topographic characteristics of a fused aluminium oxide grinding wheel. The evaluation of the grinding wheel was based on the effective contact time with the workpiece during the scratch experiment by interpreting the AE scanning signals in terms of the relative movement between the grinding wheel and an instrumented diamond tip. Rameshkumar et al. (2018) registered the acoustic emission signals in grinding operation to predict the wear level of the grinding wheel. In their investigation, the acoustic emission was analysed in time domain using different features such as root mean square, amplitude, ring-down count and average signal level. By using machine-learning techniques, for example, decision tree, artificial neural network, and support vector machine, they could estimate whether the wheel was sharp or dull. In the same way, Liao (2007) developed a grinding wheel condition monitoring method based on acoustic emission wavelet packet transform to estimate the wheel sharpness or dullness. Later, Liao (2010) developed a model based on the analysis of acoustic emission signal using autoregressive modelling and discrete wavelet decomposition to classify the state of grinding wheel. Liu et al. (2005) and (2006) determined the wavelet packet transform was an ideal signal processing method to evaluate the acoustic emission signal and to extract features correlated to the grinding burn phenomena. Similarly, Yang et al. (2014) developed a sensor system based in acoustic emission signal to extract grinding burn features, but instead of using wavelet packet transform, the Hilbert-Huang transform (HHT) was used. For the signal feature extraction, they used the average energy and the energy percentage for obtaining the HHT components correlated with the burn defects. Chiu and Guao (2008) constructed an support vector machine (SVM) model for the state classification of CBN grinding with featured data from acoustic emission signals. Dias et al. (2016) proposed a new methodology to predict and detect the surface quality and the dimensional errors by acoustic emission in centreless grinding process, where the acoustic emission was processed in both

the frequency and the time-frequency domain by fast Fourier transform and wavelet analysis, respectively.

Using acoustic emission signals in grinding process monitoring is commonly applied to assess the wear level of the grinding wheel, which is a kind of aggregation of grain shapes in the grinding wheel surface. However, the direct relationship between the acoustic emission and the surface quality of the machined workpiece in relation to grain shapes have not been studied in a good extent and more research in this field is required. Regarding to *AE* signal processing methods in grinding processes, the time direct analysis (TDA), fast Fourier transform (FFT) and wavelet transform (WT) have been explored for analysing the signal in time, frequency and time-frequency domains, respectively. Nevertheless, another important processing method singular spectrum analysis (SSA) that is frequently used in other machining processes has not been tried in abrasive processing.
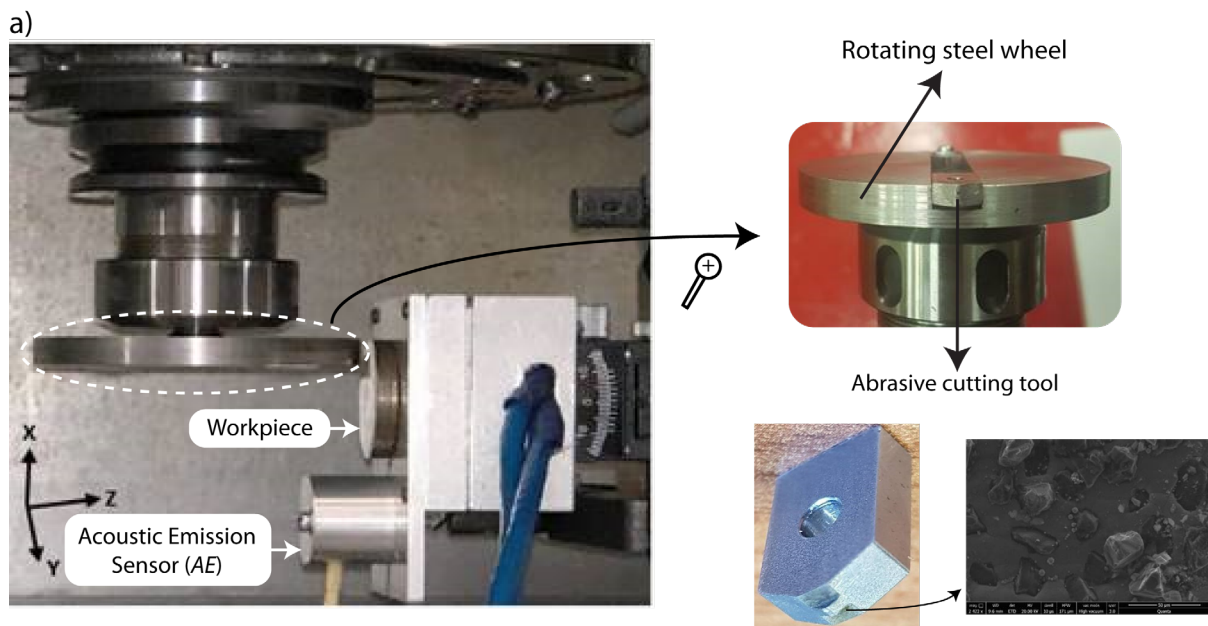
Considering aforementioned circumstances, the main objective of this study is to monitor grinding surface creation during grinding scratch tests based on the acoustic emission signals acquired. Three signal feature extraction methods are discussed here, i.e, the time direct analysis (TDA), the frequency domain analysis with the fast Fourier transform (FFT) and the analysis in the combined time-frequency domain with the singular spectrum analysis (SSA). In order to correlate the signal characterization parameters with the surface creation, multiple regression predictive models were analysed. All predictive models were analysed individually for each workpiece materials and no information about the abrasive grains were used in the models since the data source for model development is based exclusively in the acoustic emission signals.
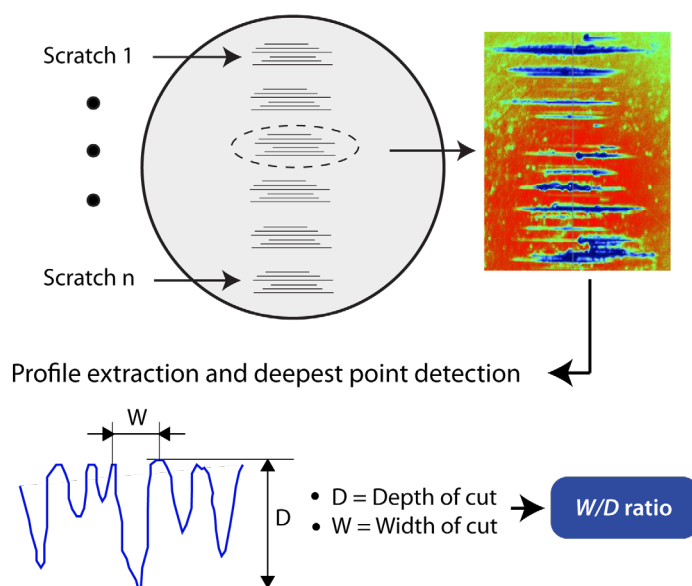
2. Experimental Design and Methodology

The abrasive scratching experiments were carried out on a numerical control machine centre XR 610 VMC Bridgeport, using abrasive cutting tools assembled to a rotating steel wheel of diameter 80 mm (see Fig. 1a). Five different types of diamond abrasives of different geometrical shapes were used for the cutting tools. The workpiece materials used in the tests were zirconia and sapphire, and their mechanical properties are shown in Table 1. The samples were prepared with surface roughness Ra 0.064 μm for zirconia and Ra 0.151 μm for Sapphire. The test sample was carefully lined up with machining plane within a 2 μm range to ensure actual depth of cut in the range of interests. An *AE* gap eliminating technique was applied to ensure the initial contact was less than 1 μm. Each test was carried out under dry condition, with a cutting speed (V_s) of 1 m/s, a downward feed rate (V_w) of 1000 mm/min and a nominal cutting depth (a_e) of 1 μm. The cutting spindle rotational speed was 238 rpm. In each machining trial, the acoustic emission (*AE*) was registered using a Physical Acoustics WD sensor mounted as near as possible to the cutting zone. *WD* is a true differential wideband sensor calibrated and certified by "Physical Acoustics Corporation" which owns a very high sensitivity and bandwidth. The optimum operating range is defined in the frequency range of 100-900 kHz and for and appropriate signal definition the sampling frequency (f_s) of 2 MHz was selected. As it is shown in Fig. 1b, each scratch surface was measured using a Bruker interferometer and the deepest cut (*D*) and its width of cut (*W*) were evaluated. The parameter selected to characterize the surface creation was the ratio *W/D*, which could be an indicator of grit shape that engaged with workpiece. The registered acoustic emission signals in each test can be extracted into individual scratch signal (Fig. 1c). This subdivision enabled the direct correlation between the acoustic emission signals and the abrasive feature values of the *W/D* parameter.

Table1: Typical ranges of mechanical properties for sapphire (Lounis Ait Ourab, 2020) and zirconia (Xiao et al., 2016) (Ma et al., 2020) materials.

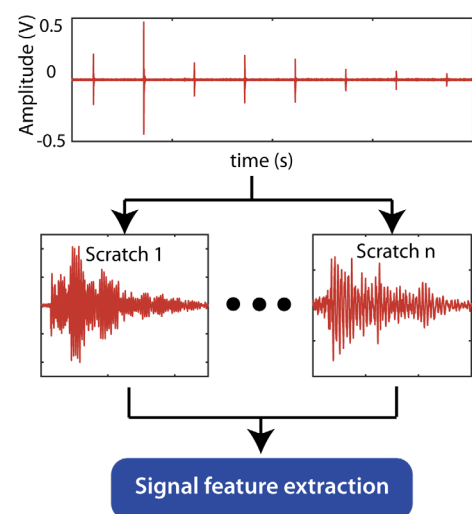| PROPERTIES	SAPPHIRE	ZIRCONIA
Tensile strength (MPa)	400	350-550
Young´s Modulus E (GPa)	345	210-220
Flexural strength (MPa)	2500 - 4000	800 - 1000
Poisson´s ratio	0.25 – 0.3	0.3
Hardness (GPa)	18-22	12-18
Density (g/cm^3)	3.98	5.8 - 6.05

Fig. 1. Experimental design.

The methodology applied in this study involved the analysis of the acoustic emission signals using the three signal feature extraction methods as shown in Fig 2. The acoustic emission signal processed with the TDA, FFT and SSA signal processing methods was statistical, characterized by the features shown in Table 2. To correlate the signal features extracted by each method with the W/D parameter, multivariable polynomic regression methods were applied as predictive techniques to assess the relation between scratch feature parameter W/D and acoustic emission characteristics. Finally, an exhaustive analysis of signal feature extraction was carried out to determine the optimum signal feature extraction for the monitoring of surface creation in relation to W/D parameter.
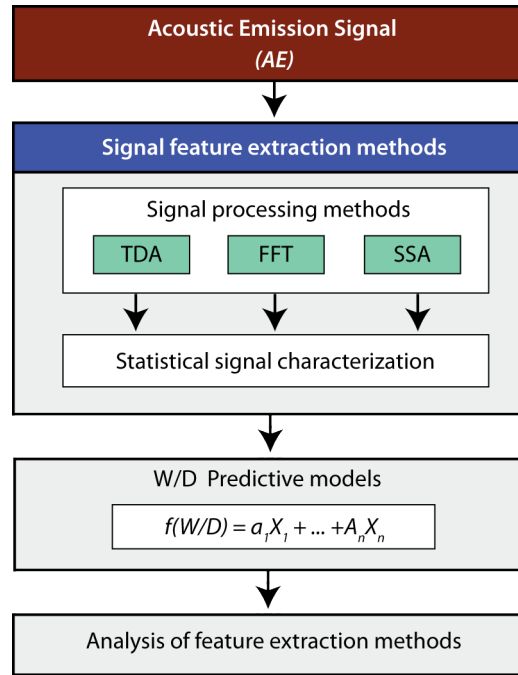

Fig. 2. Methodology.

Table 2. Statistical feature extraction of acoustic emission signal.

FEATURES	TDA	FFT	SSA
Root mean square	RMS	RMS^{fi}	$RMS^{\lambda i}$
Standard deviation	SD	SD^{fi}	$SD^{\lambda i}$
Maximum amplitude	-	A^{fi}	-
Peak to peak amplitude	PP	-	$PP^{\lambda i}$
Kurtosis	K	K^{fi}	$K^{\lambda i}$
Skewness	S	S^{fi}	$S^{\lambda i}$
Energy	E	E^{fi}	$E^{\lambda i}$
Entropy	SE	SE^{fi}	$SE^{\lambda i}$
Mean	X	X^{fi}	$X^{\lambda i}$
Frequency of maximum	-	F^{fi}	-

*Where the superscript fi indicates the frequency range ($f1,\ldots,fn$) for FFT method, the superscript λi the number of eigenvalue ($\lambda_1,\ldots,\lambda_L$) for SSA method.

All of the models obtained were diagnosed by analysing atypical values, multicollinearity, independence and normality of the residuals, homoscedasticity, and hypothesis contrast tests. The

predictive models were built using stepwise regression method, frequently used in machining process monitoring. In this technique, only significative variables are incorporated to the model and non-significative variables are rejected automatically. The method progressively introduces the signal features (one by one) into the model and it can be described as follow: in each step, a new feature is added to the model and then, **F** test are realized and p-values of all candidate variables included in the model are determined to verify if their significance decrease below the specified significance levels. If any variable is statistically non-significative, it is rejected from the model and the process continues until the last variable is analysed. This method requires two significance levels: one for adding and the other for removing features. Both levels were defined for obtaining variables with statistical significance at 90% of confidence, i.e. all features in the model have p-values lower than 0.01. The model for illustrating the relation between the scratch feature parameter *W/D* and the features of acoustic emission signals might be presented with a formula as shown in Eq.1. Predictive models were assessed in four ways. Firstly, the goodness of fit to experimental data was evaluated using the adjusted determination coefficient (adjusted R-squared, R^2_{adj}). This coefficient is a modification of R-Squared parameter (Eq.2), which consider the effect of the number of independent regressors (signal features) and evaluates how the predicted data are adjusted within the line of the regression equation. The higher the value of R^2_{adj} (Eq.3), the better model fit to the experimental data. Secondly, the sum of squares type III and the p-values (Eq.4) (Box et al., 2005) were calculated in order to determine the variables for better correlated with the *W/D* parameter. The sum of squares type III determines the effect of each significant signal feature over the response variable (*W/D*) after all other features available in the model have been considered. The sum of error squares can indicate the estimation error reduction when a new variable is added to the predictive model. The higher values in the sum of squares of a signal feature, the more influence in the response variable. The general function of the sum of squares of deviations is expressed in Eq. 5, which comprises two items on the right indicating the sum of squares of the regression model and the sum of squares of the residuals, respectively. Furthermore, the goodness of fit was evaluated by the graphical representation of the experimental values of *W/D* versus the predicted values with the predictive model. Finally, the reliability of the model was assessed by the percentage in the distribution error (e_r) (Eq. 6).

$$f(\frac{W}{D}) = a_o + \sum_{i=1}^{n} a_i x_i \ , \ i = 1,...,n \tag{1}$$

where a_i was a constant, x_i an *AE* significative features, and *n* the total number of significant features.

$$R^2 = \frac{\sum_{i=1}^{m}(\hat{y}_i - \overline{y})^2}{\sum_{i=1}^{m}(y_i - \overline{y})^2}, \ i = 1,...,m \tag{2}$$

where $\hat{y}_i$ was the predicted value of surface creation (*W/D*) at *i* observation, y_i was the experimental value of *W/D* (response variable) at *i* observation, $\overline{y}$ was the mean value of the response variable, and *m* was the total number of the *W/D* values obtained in the experimental measurements.

$$R^2_{adj} = 1 - \frac{(1-R^2)(m-1)}{m-n-1} \tag{3}$$

$$p\text{-}value = P \ (x_i \ \text{from} \ H_0 | H_0 \ \text{true}) \tag{4}$$

where *P* is a probability function and H_0 is the null hypothesis.

$$\sum_{i=1}^{m}(y_i - \overline{y})^2 = \sum_{i=1}^{m}(\hat{y}_i - \overline{y})^2 + \sum_{i=1}^{m}(y_i - \hat{y}_i)^2 \quad , \qquad i = 1, ..., m \tag{5}$$

$$e_{r_i}\left(\%\right) = \left|\frac{y_i - \overline{y}_i}{y_i}\right|100 \quad , \quad i = 1, ..., m \tag{6}$$

3. Results and Analyses

3.1 Time Direct Analysis.

The TDA is one of the most used signal processing methods in machining processes monitoring (Lauro et al., 2014). This method directly analyses the signal registered by sensors in the time domain, with no transformation or decomposition, providing fast signal processing at a low analytical-computational cost, and making it suitable for real time applications. The TDA method directly extracts the signal information using parametric characterization by statistic and non-statistics parameters (García and López, 2018). Fig. 3 shows a simulated sinusoidal signal $x(t) = \sin(wt)$ discretized by the succession $[x_i]$, with $i = 0, 1, 2, \cdots, N - 1$, and where N is the total number of points. The term N relies on sampling frequency (f_s) and sampling time (t), which has a direct impact on signal processing times. Bearing in mind, the high sampling frequency of the acoustic emission signal (f_s = 2 MHz), the sampling rate of this signal must be optimized to avoid excessive processing times incompatibles with real time applications (see Fig 3). The efficacy of the TDA method mainly depends on the type of signal, the selected features for the parametric characterization and the aspects of the machining process under assessment. In many occasions, working directly with the time domain signal parameters could provide an adequate signal characterization. However, in some cases, this method cannot extract sufficient information, which often is hidden or masked in the signal itself. The signal feature extraction using TDA method in this study is based on the parameters showed in Table 2.
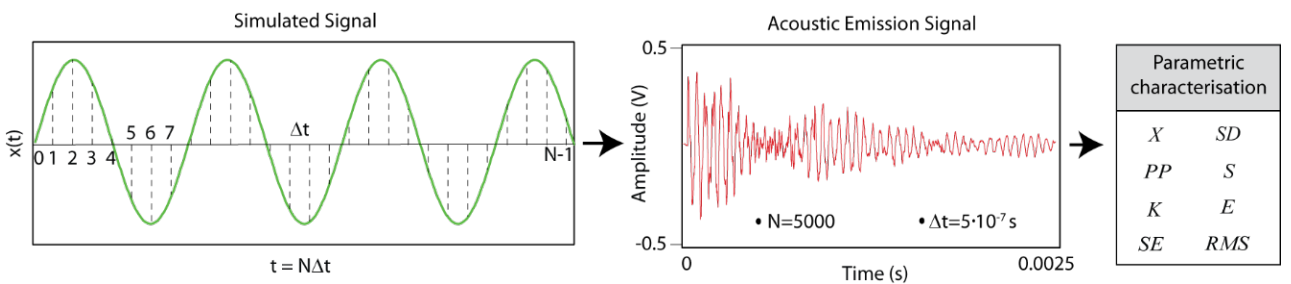

Fig. 3. Time direct analysis signal processing method.

Considering the models built by TDA method to estimate *W/D* parameter in relation to *AE* signal features, Table 3 depicts the determination coefficient (adjusted R-squared, R^2_{adj}) of the regression models, the type III sum of squares (Box et al., 2005), the p-values for the significant characterization parameters and the coefficients (a_i) of the regression model equation. For both sapphire and zirconia materials, it can be observed that the obtained predictive models give very poor results in correlation to the parameter *W/D*. The model for sapphire expressed only 10.6% of the variability of the experimental data, and the model for zirconia expressed the 25.5 %. This implies that the signal feature extraction method in time domain (TDA) failed to achieve an adequate signal characterisation.

Table 3. Significant parameters of the sapphire and zirconia predictive models for the TDA method.

Sapphire				Zirconia			
R^2_{adj} = 10.6 %				R^2_{adj} = 25.25 %			
Features	Coef. (a_i)	SS Type III	p-Value	Features	Coef. (a_i)	SS Type III	p-Value
Constant	55.17	-	-	Constant	45.7	-	-
K	-2.461	4871	0.018	RMS	-370	1611.5	0.001
Error	-	31942	-	E	1230	949.6	0.010
-	-	-	-	Error	-	5066.6	-

The analysis of the goodness of fit to the experimental data of the TDA method are shown in Fig. 4, which revealed again that TDA method failed to provide adequate signal feature extraction for the prediction of *W/D* parameter. The reliability of the models was assessed according to the distribution of the prediction errors (Fig. 4c). Estimated values of *W/D* parameter with relative errors lower than 15% ($e_r \leq 15\%$) are considered in the optimum range of prediction and estimated values with relative errors lower than 25% ($e_r \leq 25\%$) in the acceptable range of prediction. The poor behaviour observed in the acoustic emission signal processed with TDA method for both test materials, generated models with 90.4% and 47.7% of estimated data out of the acceptable range of predictions ($e_r > 25\%$) for sapphire and zirconia, respectively.
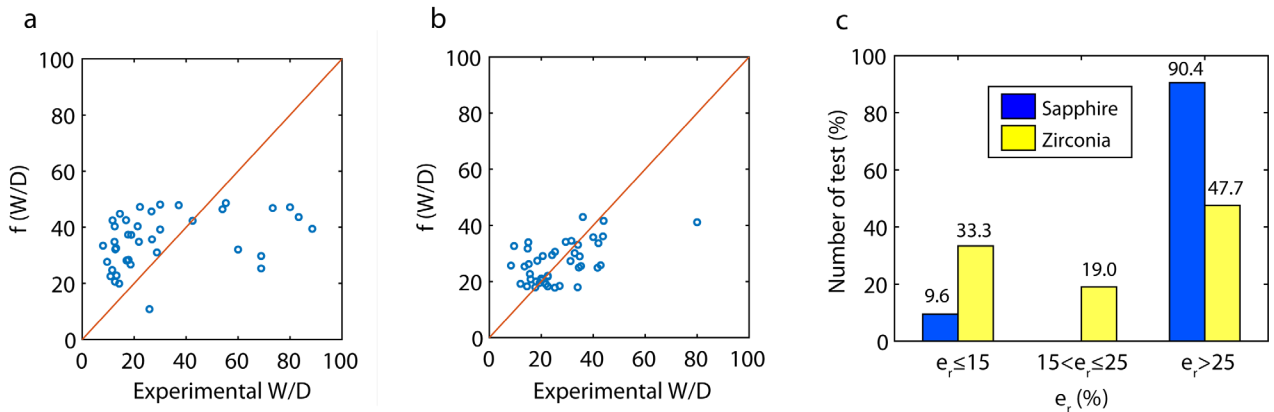

Fig. 4. Estimated values vs experimental values of the parameter *W/D* for TDA method: a) Sapphire, and b) Zirconia. c) Prediction reliability with the TDA method.

3.2 Frequency Analysis.

In the machining process monitoring, Fourier transform analysis provides the information of the frequency spectrum of monitored signals. For the succession $x[i]$ the discrete Fourier transform (DFT) was defined by Eq. 7:

$$X_k = \sum_{i=0}^{N-1} x_i e^{-j\left(\frac{2\pi ki}{N}\right)}, \quad k = 0,1,2,\ldots,(N-1)$$

(7)

The main restriction of (Eq. 7) is its high computational cost, due to the calculus of N multiplications of the term $x_i e^{-j(2\pi ki/N)}$ for each of the N values of X_k, in other words, this algorithm entails the calculation of approximately N^2. Thus, for high frequency sample signals, as acoustic emission signal is, the use of this algorithm may not be an ideal processing method. To overcome this

drawback, the DFT is implemented by using the algorithm with the highest computational efficiency denominated fast Fourier transform (FFT), which reduces the number of operations to $N \log_2 N$.

In order to determine the general behaviour of the *AE* signal in frequency domain, and establish the frequency ranges with potentially more information about the machining process, the power spectrum of *AE* signal for both the sapphire and zirconia materials are shown in Fig. 5. It can be observed similar behaviours in all diamond scratch tests with some differences in the power spectrum amplitude between the five diamond abrasives due to the differences in grain attribute and shape. The *AE* spectrum reaches the maximum amplitude at approximately 35 kHz (1). After that frequency, the power spectrum gradually decreases until around 400 kHz (2), then, a few feature peaks of power spectrum were found between 450 and 600 kHz (3).
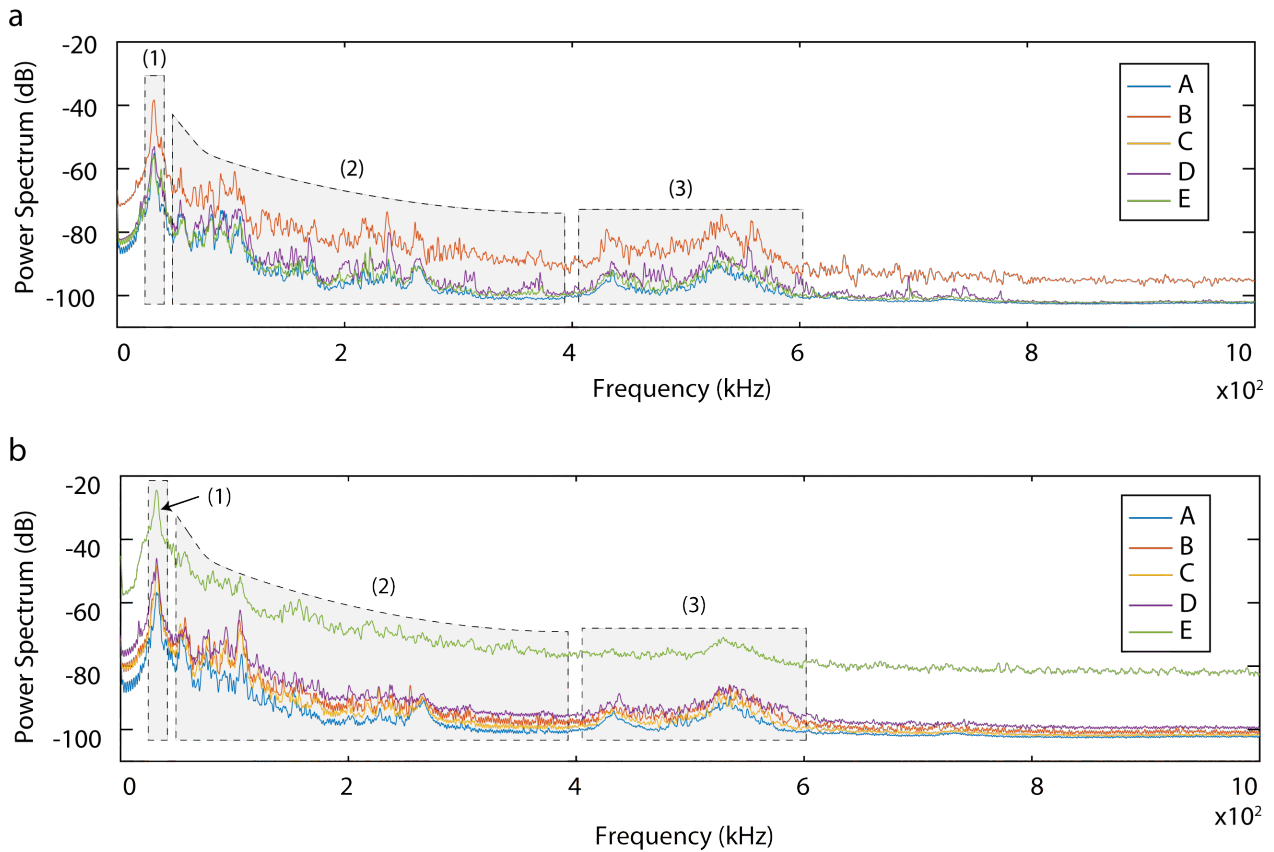

Fig. 5. Acoustic emission power spectrum: a) sapphire, and b) zirconia.

According to the preliminary analysis, it can be seen that relevant spectrum frequency range is around 0-600 kHz. The frequency analysis of *AE* signal was undertaken with a complete analysis of the bandwidth 0-600 kHz (Fig. 6a). It should be noted, that the total bandwidth under analysis entails certain frequency ranges with significant information fails to be adequately characterized, thus, the analysis was realised in two ways. Firstly, the entire bandwidth 0-600 kHz was discretized into six independent frequency ranges of 100 kHz each (Fig. 6b). Secondly, to analyse smaller frequency ranges, the bandwidth 0-600kHz was split into three independent frequency intervals of 0-200 kHz, 200-400 kHz and 400-600 kHz (Fig. 6c). To achieve a precise signal characterization, each new bandwidth was fractioned into twenty independent frequency ranges of 10 kHz each.
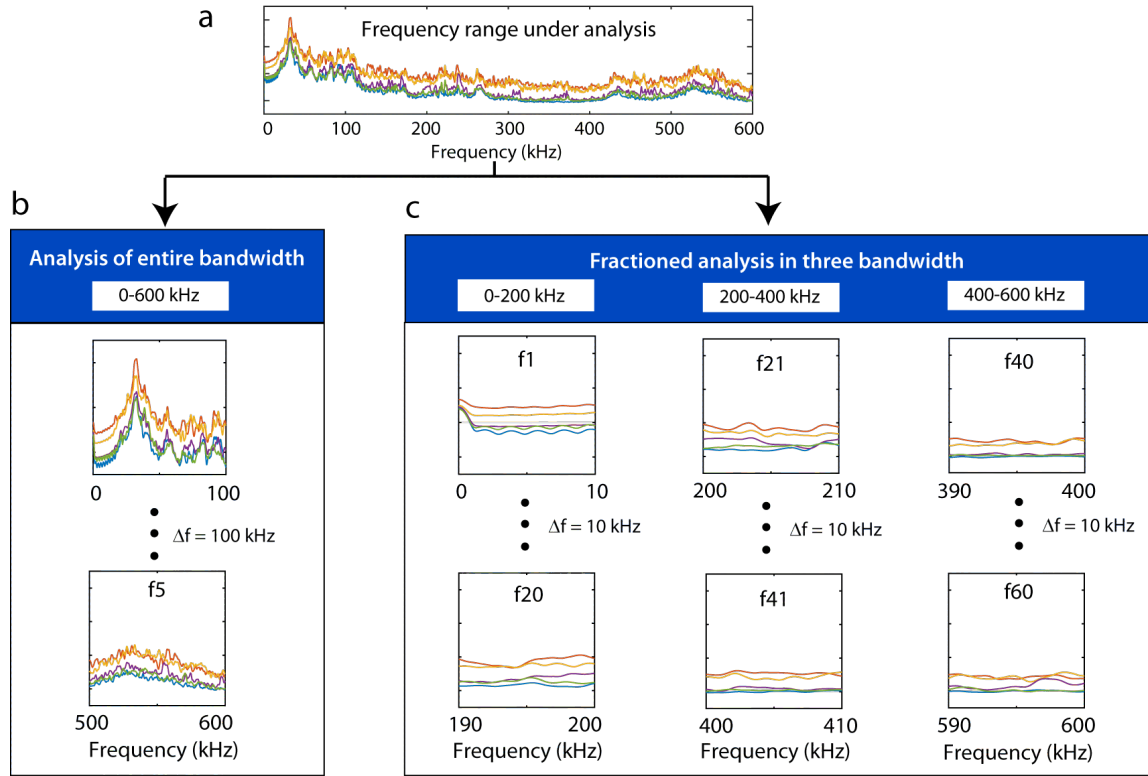
Fig. 6. Frequency ranges for *AE* signal analysis.

3.2.1 Analysis of frequency range 0-600 kHz.

The Table 4 depicts the results of the regression models for estimating *W/D* parameter by the processing of the *AE* signal in the bandwidth 0-600 kHz with FFT method, for both the sapphire and zirconia materials. Table 4 shows the determination coefficient (R^2_{adj}), the frequency ranges, the type III sum of squares, the p-values and the coefficients of the regression model equation for the significant characterization parameters.

As it was mentioned in Table 2, the superscript of the features indicates the frequency range of concerned feature variable, for example, the feature X^{f2} indicate the arithmetic mean of the FFT in the frequency range 100-200 kHz. It can be observed that both materials, obtained predictive models with very poor results, having little impact on the parameter *W/D*. The model for sapphire explained the 33.62% of the variability of the experimental data, and the model for zirconia only the 18.52 %, which indicated a very poor correlation to *W/D* parameter.

Table 4. Significant parameters of the sapphire and zirconia predictive models for the FFT method in 0-600 kHz.

Sapphire				Zirconia			
R^2_{adj} = 33.62 %				R^2_{adj} = 18.52 %			
Features	*Coef. (a_i)*	*SS Type III*	*p-Value*	*Features*	*Coef. (a_i)*	*SS Type III*	*p-Value*
Constant	73.9	-	-	*Constant*	-29.3	-	-
X^{f2}	46.5	1824	0.089	X^{f1}	-2.73	901.6	0.016
S^{f3}	-13.43	6218	0.003	E^{f5}	0.000147	491.2	0.070
SE^{f3}	-108.3	2982	0.031	*Error*	-	5522.9	-
E^{f6}	-104290	5957	0.003	-	-	-	-
Error	-	22051	-	-	-	-	-

The analysis of the goodness of fit to the experimental data of the FFT method in the entire bandwidth are shown in Fig. 7. The results were quite similar to that of TDA analysis, where the predictive models for both materials obtained poor results. The model for sapphire (Fig. 7a) overestimated the data in most of the cases for values of *W/D* parameter between 10 and 50, and underestimated the data for values of *W/D* between 50 and 90. The model for zirconia (Fig, 7b) obtained better results with homogeneous distribution, but with higher deviation in many data. In relation to model reliability in terms of the distribution error of the estimated data, once again the results showed poor behaviour, where 83.3% and 59.6% of estimated data were out of the acceptable range ($e_r > 25\%$) for the sapphire and zirconia models, respectively. This implies the analysis of the bandwidth 0-600 kHz in intervals of 100 kHz is not valid to extract significative information of *AE* signal correlated with *W/D* parameter.
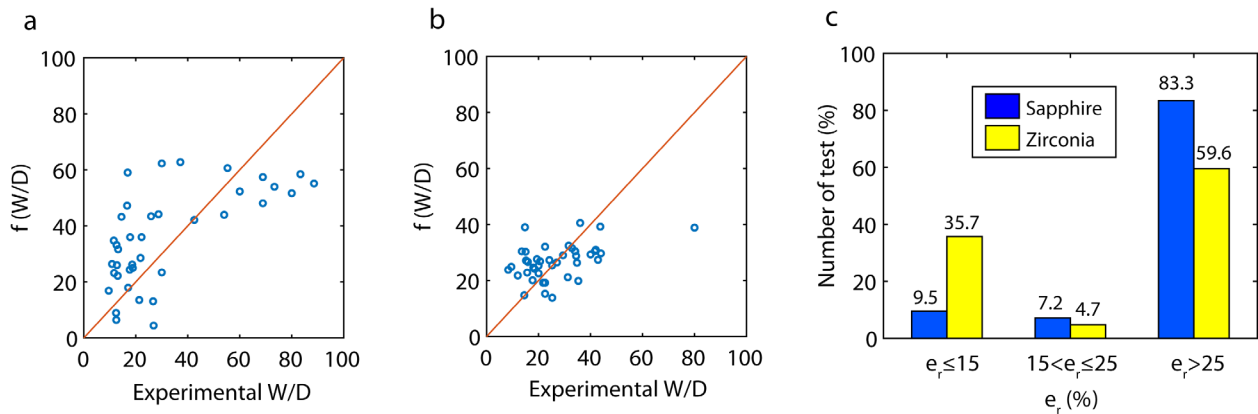

Fig. 7. Estimated values vs experimental values of the parameter *W/D* for FFT method in 0-600 kHz: a) Sapphire, b) Zirconia. c) Prediction reliability with the FFT method in 0-600 kHz.

3.2.2 Analysis of 0-200, 200-400 and 400-600 kHz in steps of 10 kHz. More precise analysis in frequency domain is needed due to the poor efficiency in predictive models of the previous analysis. Fig. 8 shows the determination coefficient (R^2_{adj}) of the predictive models built in three independent frequency bandwidths of 0-200 kHz, 200-400 kHz and 400-600 kHz, for both the sapphire and zirconia materials. As it was mentioned in the previous section, each bandwidth was fractioned into independent frequency ranges of 10 kHz to achieve a precise signal characterization. It can be observed that the determination coefficient of all models dramatically increased compared with the analysis in the bandwidth 0-600 kHz. The best results were obtained at lower frequencies (0-200 kHz), reaching predictive models with excellent fit to experimental data with R^2_{adj} of 95.5% and 90.7% for sapphire and zirconia, respectively. In the medium frequencies (200-400 kHz) the behaviour of the predictive models in both materials was totally different, the model for sapphire explained de 87.7% of the variability of the experimental data whereas the model for zirconia expressed only 54.2%. At higher frequencies (400-600 kHz) both models the sapphire and zirconia obtained similar results with R^2_{adj} of 84.2 % and 81.3%, respectively.

Table 5 shows the significative features for the best predictive models obtained in the bandwidth 0-200 kHz (see Fig. 8), for sapphire and zirconia materials. For the sapphire model, a broad number of the analysed frequency bands showed significative information correlated with the parameter *W/D*. The ranges f4 (30-40 kHz) provided the most significative feature of the model (A^{f4}) with the highest sum of square. This frequency range correspond with the higher power spectrum of the *AE* signal (see Fig 5). The next frequency bands providing high values of sum of square were in decreasing order f9 (S^{f9}), f3 (A^{f3}, S^{f3}), f20 (SE^{f20}) f14 (K^{f14}) f16 (SE^{f16}). The rest of significant frequency ranges also provided information but to a lesser extent. Similar to sapphire, the model of zirconia possesses a

broad number of analysed frequency ranges with the information correlated with the *W/D* parameter. However, in contrast, the model for zirconia presents less differences in the sum of squares of the significative features, only in the range f16 (F^{f16}) a value is slightly higher than in the rest of the variables.

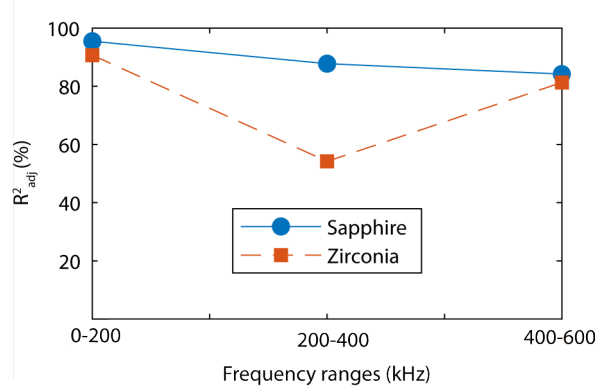

Fig. 8. Adjusted R-Squared (R^2_{adj}) obtained in the prediction of *W/D* parameter in three independent frequency intervals.

Table 5: Significant parameters of the sapphire and zirconia predictive models for the FFT method in 0-200 kHz.

Sapphire				Zirconia			
R^2_{adj} = 95.48 %				R^2_{adj} = 90.07 %			
Features	*Coef. (a_i)*	*SS Type III*	*p-Value*	*Features*	*Coef. (a_i)*	*SS Type III*	*p-Value*
Constant	-1134	-	-	*Constant*	180.6	-	-
A^{f3}	-3.289	8779.6	0.000	K^{f1}	-3.494	556.9	0.000
S^{f3}	10.33	876.8	0.000	SE^{f2}	0.0610	166.3	0.005
A^{f4}	2.237	10797.7	0.000	S^{f5}	-7.22	221.6	0.001
X^{f5}	5.67	302.9	0.011	K^{f6}	-3.735	353.6	0.000
A^{f6}	-4.194	2754.1	0.000	F^{f6}	-0.001001	169.7	0.004
F^{f6}	0.006697	4189.0	0.000	E^{f9}	-517	389.0	0.000
SD^{f8}	31.26	2140.2	0.000	SD^{f10}	7.21	493.6	0.000
S^{f9}	-53.01	9021.8	0.000	RMS^{f14}	-131.3	655.5	0.000
K^{f11}	8.682	3324.4	0.000	X^{f14}	194.3	922.0	0.000
K^{f13}	7.76	2149.6	0.000	K^{f15}	-4.568	491.3	0.000
K^{f14}	-16.89	6879.5	0.000	F^{f15}	-0.000934	176.4	0.004
SE^{f16}	28.56	5887.5	0.000	F^{f16}	-0.002430	1472.2	0.000
A^{f17}	9279	883.9	0.000	SD^{f19}	-161.0	824.3	0.000
E^{f18}	0.004789	214.2	0.030	A^{f20}	47.2	366.8	0.000
F^{f18}	-382.5	1570.6	0.000	X^{f20}	-147.4	787.2	0.000
SE^{f20}	-29.62	7163.6	0.000	F^{f20}	0.002294	804.8	0.000
Error		1013.6	-	*Error*		431.6	-

The analysis of the correlations of the estimated data versus the experimental data for the FFT method in the 0-200 kHz frequency band (Fig. 9) revealed the model for zirconia had an even

distribution in all of the *W/D* parameter ranges, with no bias and a very strong correlation (see Fig 9b). The model obtained for sapphire (Fig 9a), in spite of having higher determination coefficient than zirconia model, showed a higher deviation with underestimation of *W/D* values between 10 and 20. In the prediction error distribution of the estimated data, Fig. 9c showed the zirconia model achieved the best behaviour in all ranges of relative error under study. The model for zirconia reached a 71.4 % of estimated data in the interval of optimum prediction $(e_r \leq 15\%)$ versus the 57.1% for the sapphire model. As for the range of acceptable prediction $(e_r \leq 25\%)$, once again the model for zirconia expressed the best results with a 95.2 % of estimated data versus the 76.2% for the sapphire model.
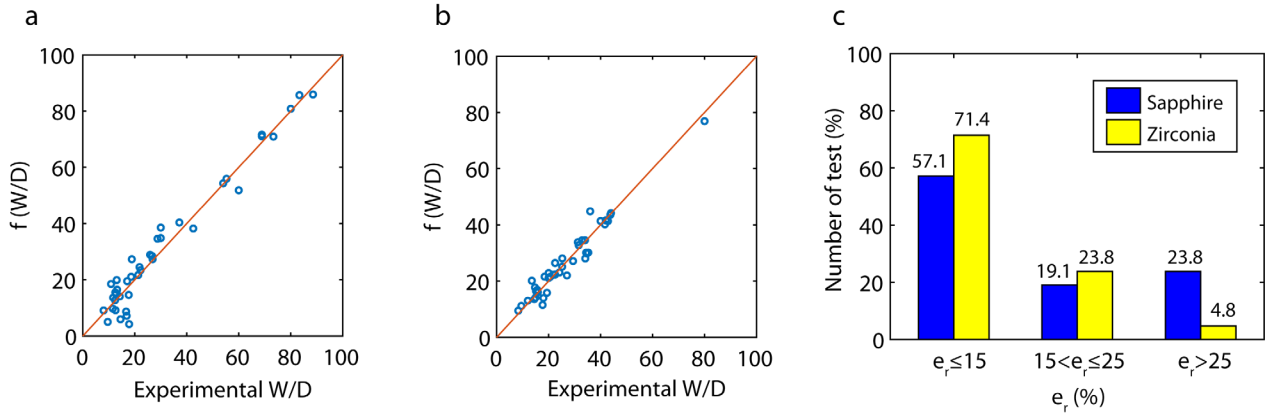

Fig. 9. Estimated values vs experimental values of the parameter *W/D* for FFT method in 0-200 kHz: a) sapphire. b) zirconia. Prediction reliability with the FFT method in 0-200 kHz.

According to the analysis above, the bandwidth 0-200 kHz discretized in frequency ranges of 10 kHz was the best method to obtain an optimal acoustic emission signal characterisation in the FFT analysis. This method provided an optimal correlation between the acoustic emission signal and the *W/D* parameter in both materials, reaching for the zirconia material a slightly better behaviour. The proposed method enabled to obtain the frequency ranges with the most significative information of the process. In addition, the signal processing only in the bandwidth 0-200 kHz implies that the sample frequency of the acoustic emission could be substantially reduced, improving the computational cost and making this method suitable for real time applications.

3.3. Singular Spectrum Analysis

As it was mentioned in the introductory section, singular spectrum analysis (SSA) is a common signal processing method frequently used in machining process monitoring, however, it has never been applied to surface creation supervision in abrasive scratch experiment considering *AE* signal. SSA is an advanced non-parametric signal processing method that enables the signal analysis in the combined time-frequency domain. SSA method transforms a time signal into an independent time series with defined frequency ranges referred to as the principal component as illustrated in Fig. 10. The mathematical development of the SSA technique described by Golyandina et al. (2001) can be split basically in four steps: the first step consists of the calculate of a Hankel matrix $\mathbf{X} = (X_i,..., X_{K-1})$ from the original signal registered by the sensor $x = (x_0,...,x_{N-1})$, where N is the number of point of the sample. This matrix is commonly referred to as the trajectory matrix, with $X_i = (x_{i-1},...,x_{i+L-2})^T$, $1 \leq i \leq K$ and $K = N - L + 1$, where L is an integer number denominated window length. The second step is to calculate the singular value decomposition (SVD) of the trajectory matrix decomposing the X matrix into a series of elementary matrixes $X_i = \sqrt{\lambda_i} U_i V_i^T$,

with $V_i = X^T U_i / \sqrt{\lambda_i}$, and where U_i and λ_i are the eigenvectors and eigenvalues of the matrix $S = XX^T$. In the third step, the time series reconstruction of the elementary matrixes X_i is performed using the individual or the grouped reconstruction method (García and Núñez, 2017). The individual method is applied when there is no correlation between matrixes X_i, and the grouped method is applied when there is a correlation among them. This method permits the reduction of principal components, and analytical-computational cost by defining a grouping indices I_k, with $k = 1, ..., m$, in such a way that the trajectory matrix can be represented by the expression

$$X = \sum_{k=1}^{m} X_{I_k} \tag{8}$$

Finally, in the fourth step, each matrix X_{I_k} is transformed into a time series $g_k = (g_k^1, g_k^2, g_k^3)$ of length N termed principal component, where g_k^1 calculates the elements of a series for $0 \leq k < L^* - 1$ using Eq.9, g_k^2 for $L^* - 1 \leq k < K^*$ through Eq.10, and g_k^3 for $K^* \leq k < N$ with Eq.11 (García and Núñez, 2017).

$$g_k^1 = \frac{1}{k+1} \sum_{m=1}^{k+1} x_{m,k-m+2}^* \tag{9}$$

$$g_k^2 = \frac{1}{L^*} \sum_{m=1}^{L^*} x_{m,k-m+2}^* \tag{10}$$

$$g_k^3 = \frac{1}{N-k} \sum_{m=k-K^*+2}^{N-K^*+1} x_{m,k-m+2}^* \tag{11}$$

where $L^* = \min(L, K)$ and $K^* = \max(L, K)$.

As it was mentioned previously, each principal component obtained in the signal decomposition of the original signal with the SSA method is associated to a specific frequency range, which enables the method the real-time ability for advanced signal filtering with combined time-frequency characterization (Fig. 10).

The window length (L) is a crucial factor to achieve an optimum signal decomposition with the SSA method. The adequate selection of this parameter depends mainly on the type of signal and the machining process under study. If the window length is too narrow, the analysis is simplified due to the lower number of principal components, consequently it may lead to deficient signal decomposition with no significative information about the process. Conversely, if the window length is too long, the high number of principal components may hinder the identification of components with significative information correlated with the machining process. In this study, in order to achieve an adequate signal decomposition, predictive models were built increasing the size of the window length (L) according to the series $L = [i, 2i, 3i, ..., ni]$ were $i = 5$ and $n \in \square = \{1, 2, 3, ...\}$, stopping the process when an optimum data fit R^2_{adj} was reached. Finally, if the effective window length and the significative principal components are selected optimally, the result would be similar to other time-frequency signal processing methods such as wavelet packet transform, Hilbert-Huang transform, and principal component analysis.

Fig. 11 shows the evolution in the fit to experimental data (R^2_{adj}) for seven predictive models built with seven different window lengths, from $L=5$ to $L=35$ in steps of 5. It can be observed that at lower window lengths the SSA method failed to achieve good results with R^2_{adj} values, which are lower than 50% for both the sapphire and zirconia materials. For $L=30$, the sapphire started to improve the data fit with an R^2_{adj} of 70.1 % whereas the zirconia remained almost constant regarding to the previous window lengths. For $L=35$, both materials reached models with an optimum fit to experimental data, with R^2_{adj} of 92.3% and 96.4% for sapphire and zirconia, respectively, which means the principal components calculated at this window length provide significative information correlated with the W/D parameter.
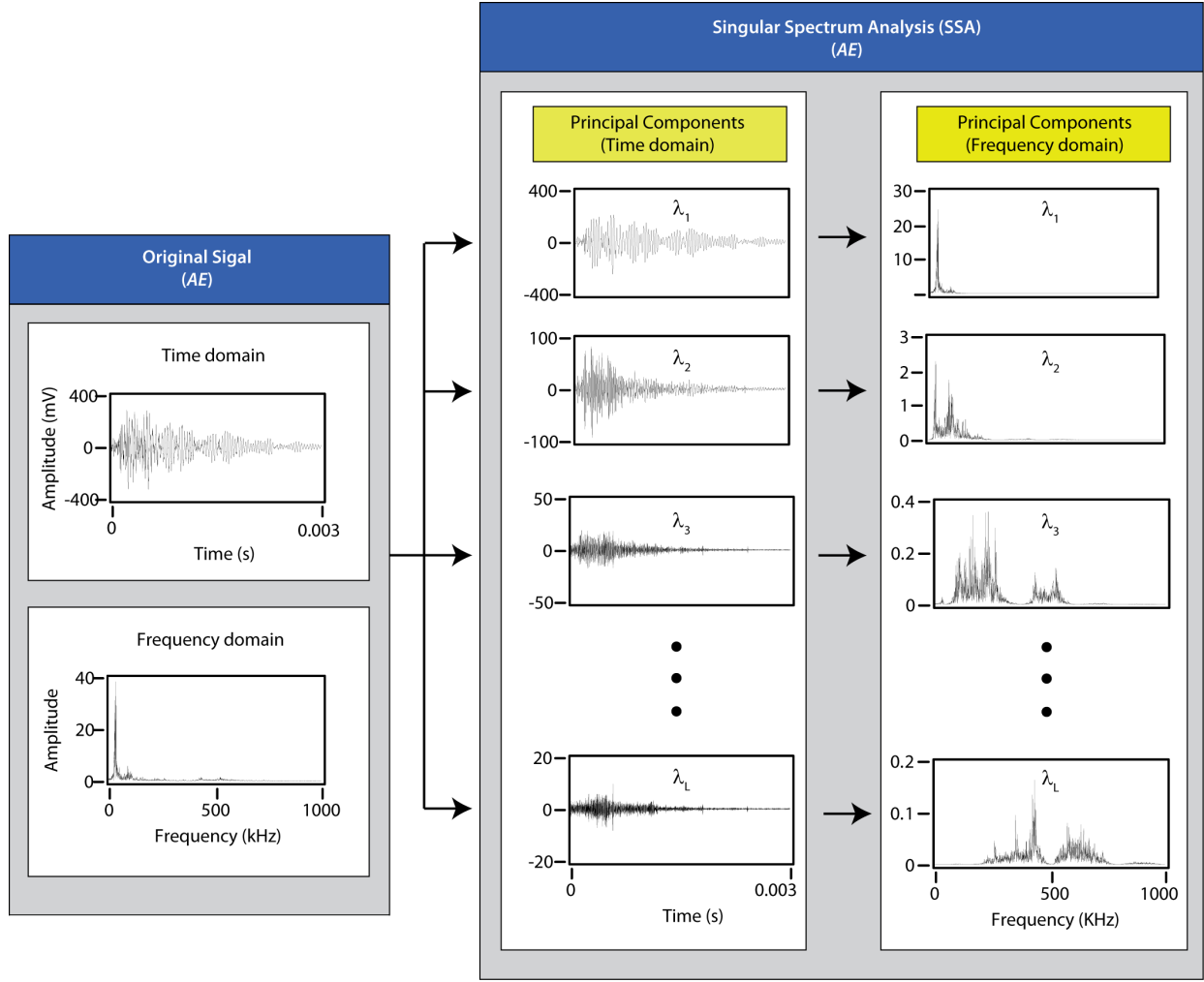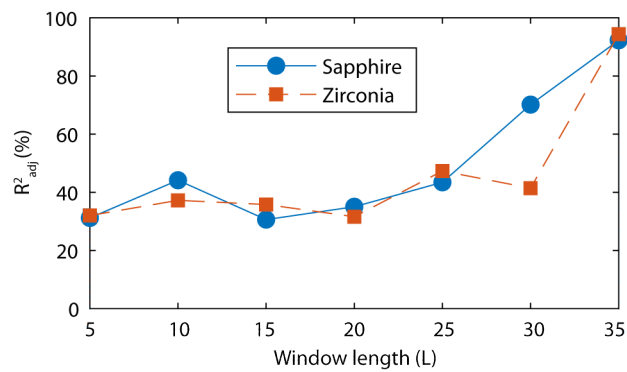
Fig. 10. SSA decomposition of a time series.

Fig 11. Adjusted R-Squared (R^2_{adj}) for different level decomposition: $L5$, $L10$, $L15$, $L20$, $L35$, $L30$ and $L35$.

Table 6 shows the principal components and the significative features for the predictive models obtained with the SSA method using a windows length of L=35. For both models, a broad number of principal components showed significative information correlated with the parameter W/D. For sapphire model, the principal components $\lambda 15$ ($K^{\lambda 15}$), $\lambda 19$ ($S^{\lambda 19}$) and $\lambda 21$ ($X^{\lambda 21}$) provided the most significative features of the model with the highest sum of square. The next frequency bands

providing high values of sum of square were in decreasing order $\lambda11$ ($X^{\lambda11}$), $\lambda32$ ($S^{\lambda32}$), $\lambda15$ ($K^{\lambda15}$), $\lambda6$ ($S^{\lambda6}$), $\lambda30$ ($S^{\lambda30}$) and $\lambda16$ ($SD^{\lambda16}$). The rest of significant principal components also provided information but in a lesser extent. In contrast with the model for sapphire, for zirconia model higher differences in the sum of squares of the significative features were not found, obtained for the principal components $\lambda7$ ($S^{\lambda7}$), $\lambda8$ ($K^{\lambda8}$), $\lambda8$ ($S^{\lambda28}$), $\lambda28$ ($PP^{\lambda28}$), $\lambda18$ ($X^{\lambda18}$) and $\lambda10$ ($K^{\lambda10}$) the most significative features. Such difference may relate to the different attributes of materials.

Table 6: Significant parameters of the sapphire and zirconia predictive models for the SSA method.

Sapphire				Zirconia			
R^2_{adj} = 92.29 %				R^2_{adj} = 96.42 %			
Feat.	*Coef.* (a_i)	*SS Type III*	*p-Value*	*Feat.*	*Coef.* (a_i)	*SS Type III*	*p-Value*
Constant	52.12		0,000	*Constant*	54.93		0,000
$SE^{\lambda1}$	0.000120	809.0	0.003	$X^{\lambda6}$	-9.56	59.47	0,005
$S^{\lambda4}$	191.9	1087.3	0.001	$S^{\lambda7}$	-1.872	1868.85	0,000
$S^{\lambda6}$	214.9	3018.0	0.000	$S^{\lambda8}$	-930.0	1480.76	0,000
$X^{\lambda11}$	110.6	6190.3	0.000	$K^{\lambda8}$	1.4120	1554.34	0,000
$K^{\lambda12}$	1.161	1457.6	0.000	$S^{\lambda10}$	-132.1	436.52	0,000
$SE^{\lambda14}$	-2.184	466.0	0.017	$K^{\lambda10}$	0.7467	1207.01	0,000
$SE^{\lambda15}$	740.6	12277.2	0.000	$P^{\lambda11}$	0.780	224.73	0,000
$K^{\lambda15}$	-2.067	3299.2	0.000	$S^{\lambda11}$	96.24	717.66	0,000
$SD^{\lambda16}$	-105.2	2970.2	0.000	$K^{\lambda15}$	-0.275	409.91	0,000
$S^{\lambda19}$	-527.0	9382.2	0.000	$X^{\lambda18}$	-160.9	1385.80	0,000
$X^{\lambda21}$	-477.7	8702.4	0.000	$SD^{\lambda19}$	-80.3	352.85	0,000
$S^{\lambda27}$	117.2	1576.3	0.000	$S^{\lambda22}$	17.39	57.46	0,006
$X^{\lambda29}$	1029	2204.4	0.000	$PP^{\lambda23}$	6.275	668.66	0,000
$S^{\lambda30}$	0.3341	3103.1	0.000	$S^{\lambda25}$	8.94	110.94	0,000
$S^{\lambda31}$	-24641	1812.9	0.000	$S^{\lambda27}$	51.15	418.45	0,000
$S^{\lambda32}$	51409	5300.3	0.000	$X^{\lambda28}$	287.3	511.09	0,000
$X^{\lambda33}$	745	469.2	0.017	$PP^{\lambda28}$	-8.166	1432.24	0,000
$S^{\lambda34}$	-51119	2063.2	0.000	$S^{\lambda34}$	-1221	72.14	0,003
$X^{\lambda35}$	-883	2167.5	0.000	$S^{\lambda35}$	5796	31.97	0,034
$S^{\lambda35}$	53492	386.6	0.028	*Error*	-	136.99	
Error	-	1454.2	-	-	-	-	-

The analysis of the goodness of fit by the correlations of the estimated data versus the experimental data for the SSA method are shown in Fig. 12. It can be observed the model for zirconia (Fig. 12b) obtained a uniform distribution with no bias in all of the ranges of *W/D* parameter. The model obtained for sapphire (Fig 12a) showed higher deviation in most of estimated values of *W/D* parameter regarding the zirconia model, underscoring two point of over-estimation highlighted in red colour. In relation to model reliability in terms of the distribution error of the estimated data, Fig. 12c showed the zirconia model achieved the best behaviour with the 92.8 % of data in the optimum range $(e_r \leq 15\%)$, and all of the data in the range of acceptable predictions $(e_r \leq 25\%)$. The behaviour for

sapphire model was totally different with only the 47.6% of data in the optimum range $(e_r \leq 15\%)$ and the 64.3% in the range of acceptable prediction $(e_r \leq 25\%)$.
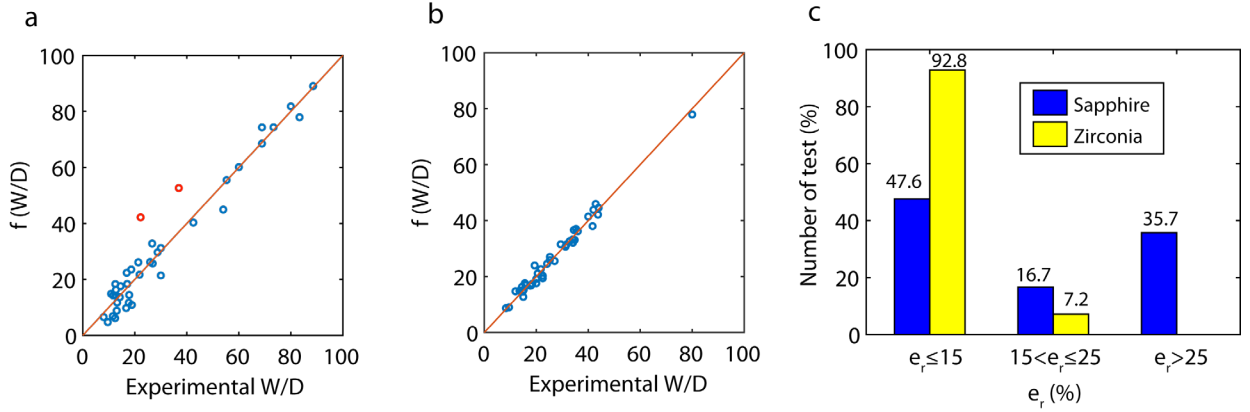

Fig. 12. Estimated values vs experimental values of the parameter *W/D* for SSA method in 0-200 kHz: a) sapphire. b) zirconia. Prediction reliability with the SSA method.

4. Conclusive Remarks

In this study, the acoustic emission signals in the abrasive scratching are analysed for surface creation monitoring by using three feature extraction methods, which are in time domain (TDA), in frequency domain (FFT) and in the combination of time-frequency domains (SSA). The surface creation was evaluated by using the scratch feature parameter *W/D* of the maximum depth scratch in the scratch profile. The analyses show:

- It has been observed that the TDA signal processing method failed to obtain meaningful signal feature extraction with coefficient of determination R^2_{adj} lower than 30%.
- For the FFT signal processing method, the analysis of the frequency range of 0-600 kHz does not provide good results due to the length of the discretization intervals (100 kHz) is too long, leaving the significative information hidden or disguised behind the signal appearance. The best bandwidth for relevant *AE* signal feature extraction was achieved at 0-200 kHz, with predictive models reaching R^2_{adj} values of 95% and 90% for sapphire and zirconia, respectively. The frequency range discretization with intervals of 10 kHz enabled the isolation and location of signal characteristics to aggregate effective information for the monitoring of the *W/D* parameter.
- For the SSA signal processing method, the best results were obtained with *L*=35, providing predictive models with R^2_{adj} values of 92% and 96% for sapphire and zirconia, respectively. The principal components providing most relevant information for monitoring the ratio *W/D* were λ15, λ19 and λ21 for sapphire, whereas no particular principal component stood out for zirconia.

Both FFT and SSA methods proved to be effective methods for *W/D* feature monitoring, whereas the best predictive model for zirconia material was obtained with SSA, the best signal processing method for sapphire material was the FFT. Nevertheless, the use of the FFT at lower frequencies (0-200 kHz) implies a great reduction in the sampling frequency of the acoustic emission signal, reducing the computational cost and making this method the most suitable for real time applications.

Finally, the research has demonstrated that acoustic emission signal in frequency domain has proven to be the most effective information for monitoring the surface creation in abrasive scratch experiments. The applicable models developed in this research provide good evidence for using *AE* signal to present abrasive machining performance in relation to abrasive physical conditions. Such knowledge could help engineers to monitor and improve grinding operations.

References

Arun, A., Rameshkumar, K., Unnikrishnan, D., Sumesh, A., 2018. Tool Condition Monitoring of Cylindrical Grinding Process Using Acoustic Emission Sensor. Mater. Today Proc. 5, 11888–11899.

Boaron, A., Weingaertner, W.L., 2018. Dynamic in-process characterization method based on acoustic emission for topographic assessment of conventional grinding wheels. Wear 406–407, 218–229.

Box, G.E.P., Hunter, J.S., Hunter, W.G., 2005. Statistics for experimenters : design, innovation, and discovery. Wiley-Interscience.

Chiu, N.H., Guao, Y.Y., 2008. State classification of CBN grinding with support vector machine. J. Mater. Process. Technol. 201, 601–605.

Dias, E.A., Pereira, F.B., Ribeiro Filho, S.L.M., Brandão, L.C., 2016. Monitoring of through-feed centreless grinding processes with acoustic emission signals. Meas. J. Int. Meas. Confed. 94, 71–79.

García Plaza, E., Núñez López, P.J., 2017. Surface roughness monitoring by singular spectrum analysis of vibration signals. Mech. Syst. Signal Process. 84, 516–530.

García Plaza, E., Núñez López, P.J., 2018a. Application of the wavelet packet transform to vibration signals for surface roughness monitoring in CNC turning operations. Mech. Syst. Signal Process. 98, 902–919.

García Plaza, E., Núñez López, P.J., 2018b. Analysis of cutting force signals by wavelet packet transform for surface roughness monitoring in CNC turning. Mech. Syst. Signal Process. 98, 634–651.

García Plaza, E., Núñez López, P.J., Beamud González, E.M., 2018. Multi-sensor data fusion for real-time surface quality control in automated machining systems. Sensors (Switzerland) 18.

Golyandina, N., Nekrutkin, V.V. (Vladimir V., Zhigliãv̄skiĭ, A.A. (Anatoliĭ A., 2001. Analysis of time series structure : SSA and related techniques. Chapman & Hall/CRC.

Griffin, J., Chen, X., 2009. Characteristics of the acoustic emission during horizontal single grit scratch tests: Part 1 characteristics and identification. Int. J. Abras. Technol. 2, 25–42.

Karam, S., Teti, R., 2013. Wavelet transform feature extraction for chip form recognition during carbon steel turning. Procedia CIRP 12, 97–102.

Lauro, C.H., Brandão, L.C., Baldo, D., Reis, R.A., Davim, J.P., 2014. Monitoring and processing signal applied in machining processes - A review. Meas. J. Int. Meas. Confed. 58, 73–86.

Lee, D.E., Hwang, I., Valente, C.M.O., Oliveira, J.F.G., Dornfeld, D.A., 2006. Precision manufacturing process monitoring with acoustic emission. Int. J. Mach. Tools Manuf. 46, 176–188.

Liu, Q., Chen, X., Gindy, N., 2005. Fuzzy pattern recognition of AE signals for grinding burn. Int. J. Mach. Tools Manuf. 45, 811–818.

Liu, Q., Chen, X., Gindy, N., 2006. Investigation of acoustic emission signals under a simulative environment of grinding burn. Int. J. Mach. Tools Manuf. 46, 284–292.

Lounis Ait Ourab, 2020. Micron Diamond Processing of Advanced Ceramics. PhD Thesis, Liverpool John Moores University..

Ma, Z., Wang, Z., Wang, X., Yu, T., 2020. Effects of laser-assisted grinding on surface integrity of

zirconia ceramic. Ceram. Int. 46, 921–929.

Nguyen, D.T., Yin, S., Tang, Q., Son, P.X., Duc, L.A., 2019. Online monitoring of surface roughness and grinding wheel wear when grinding Ti-6Al-4V titanium alloy using ANFIS-GPR hybrid algorithm and Taguchi analysis. Precis. Eng. 55, 275–292.

Siddhpura, M., Paurobally, R., 2012. A review of chatter vibration research in turning. Int. J. Mach. Tools Manuf. 61, 27–47.

Tang, J., Du, J., Chen, Y., 2009. Modeling and experimental study of grinding forces in surface grinding. J. Mater. Process. Technol. 209, 2847–2854.

Teti, R., Jemielniak, K., O'Donnell, G., Dornfeld, D., 2010. Advanced monitoring of machining operations. CIRP Ann. - Manuf. Technol. 59, 717–739.

Warren Liao, T., 2010. Feature extraction and selection from acoustic emission signals with an application in grinding wheel condition monitoring. Eng. Appl. Artif. Intell. 23, 74–84.

Warren Liao, T., Ting, C.F., Qu, J., Blau, P.J., 2007. A wavelet-based methodology for grinding wheel condition monitoring. Int. J. Mach. Tools Manuf. 47, 580–592.

Wegener, K., Hoffmeister, H.W., Karpuschewski, B., Kuster, F., Hahmann, W.C., Rabiey, M., 2011. Conditioning and monitoring of grinding wheels. CIRP Ann. - Manuf. Technol. 60, 757–777.

Weingaertner, W.L., Boaron, A., 2012. A method to determine the grinding wheel's topography based on acoustic emission. Int. J. Abras. Technol. 5, 17–32.

Xiao, X., Zheng, K., Liao, W., Meng, H., 2016. Study on cutting force model in ultrasonic vibration assisted side grinding of zirconia ceramics. Int. J. Mach. Tools Manuf. 104, 58–67.

Yang, M., Li, C., Zhang, Y., Jia, D., Li, R., Hou, Y., Cao, H., Wang, J., 2019. Predictive model for minimum chip thickness and size effect in single diamond grain grinding of zirconia ceramics under different lubricating conditions. Ceram. Int. 45, 14908–14920.

Yang, Z., Yu, Z., Xie, C., Huang, Y., 2014. Application of Hilbert-Huang Transform to acoustic emission signal for burn feature extraction in surface grinding process. Meas. J. Int. Meas. Confed. 47, 14–21.